Journal of Materials and Environmental Science
ISSN : 2028-2508
e-ISSN : 2737-890X
CODEN : JMESCN

J. Mater. Environ. Sci., 2025, Volume 16, Issue 9, Page 1684-1696

http://www.jmaterenvironsci.com

Design and Characterization of Hybrid Phase Change Material: Paraffin Wax Enhanced with Copper Oxide Nanoparticles for Improving the Thermo-Electrical Performance of Solar Panels

Abdulrazzaq Hammal[1] *, Bahia Sheikh Al-Qassabeen[2], Khaldoun Hafez[3]

[1]*Department of Basic Sciences, Faculty of Electrical and Electronic Engineering, University of Aleppo*

[2]*Master's Student, Department of Environmental Engineering Technologies, Faculty of Technical Engineering, University of Aleppo*

[3]*Department of Environmental Engineering Technologies, Faculty of Technical Engineering, University of Aleppo*

**Corresponding author, Email address: hammal1986@gmail.com*

Received *22 July 2025,*
Revised *24 Aug 2025,*
Accepted *26 Aug 2025*

Keywords:

- ✓ *Phase-change materials*
- ✓ *Solar cells cooling systems*
- ✓ *Renewable energy*
- ✓ *Thermal conductivity*

Citation: *Hammal A., Bahia Sheikh Al-Qassabeen B.S., Khaldoun Hafez K. (2025), Design and characterization of hybrid phase change material: paraffin Wax enhanced with copper oxide Nanoparticles for Improving the thermo-Electrical performance of Solar panels, J. Mater. Environ. Sci., 16(9), pp. 1684-1696*

Abstract: In this research, an integrated system was developed to enhance the performance of photovoltaic cells through the design of a highly efficient hybrid phase-change material. The work began with the preparation of copper oxide nanoparticles (CuO NPs) using the chemical precipitation method. Analyses using X-ray diffraction (XRD) and atomic force microscopy (AFM) confirmed their high purity and crystalline regularity, with sizes ranging between 18-25 nm. These nanoparticles were then incorporated at 2% by weight into paraffin wax to prepare the hybrid material, which showed significant improvement in thermal properties, represented by a 381.8% increase in thermal conductivity compared to pure paraffin wax. When this hybrid material was applied as a cooling system for photovoltaic panels, notable performance improvements were observed, including an average reduction in cell temperature of 14.4°C, leading to a 29.11% increase in maximum power output (from 28.82 W to 37.21W) at peak solar irradiance, and an improvement in energy conversion efficiency from 9.4% to 12.18%. The system also achieved a 22.75% increase in daily energy productivity. These improvements are attributed to the formation of effective thermal conductive networks within the paraffin wax and enhanced efficiency in latent heat absorption and release. These results confirm the successful preparation of an innovative cooling system using nano-enhanced phase-change materials, offering a practical and effective solution to heat-related problems in solar cells, with promising potential for large-scale industrial applications in renewable energy systems.

1. Introduction

Amid the global transition toward sustainable energy systems, photovoltaic (PV) panels face critical efficiency challenges due to thermal rise, which causes significant energy loss. PV cells absorb 80–85% of solar radiation, converting it into waste heat rather than electrical energy (Soudi *et al.* 2020). This effect manifests clearly in a 0.5% reduction in open-circuit voltage (*V*_{oc}) per degree Celsius above the nominal temperature (25°C), a problem exacerbated in hot climates where panel temperatures can reach 70°C during summer.

To address this issue, three primary heat management strategies have emerged:

Phase Change Materials (PCMs), which utilize latent heat of phase transition to absorb excess thermal energy (Baloch *et al.* 2015; Haidar *et al*. 2018; Han *et al*. 2016; Dwivedi *et al*. 2020).

Hybrid cooling systems integrating water-based or air-based cooling with PCMs.
Thermochemical Heat Storage (TCHS) systems employing materials such as hydrated salts (Domański & Rebow, 1995).
These technologies have demonstrated the ability to enhance solar system efficiency by 15–20% (Tewari & Dev, 2018; Pal *et al*. 2018; Rouf *et al*., 2016; Armstrong & Hurley, 2010), despite ongoing challenges in developing low-cost materials and smart infrastructure (Byiringiro *et al*., 2025; Stritih, 2016; Rajaram & Sivakumar, 2015; Indartono *et al*. 2016).
Thermal energy storage serves as a fundamental solution for maximizing renewable energy utilization, classified into three types:

1. **Sensible Heat Storage (SHS)**, involving temperature change without phase transition.
2. **Latent Heat Storage (LHS)**, leveraging energy from phase transitions.
3. **Thermochemical Heat Storage (TCHS)**, relying on reversible chemical reactions.

LHS systems exhibit superior storage capacity (Huang *et al*. 2011; Khanna *et al*. 2018), making them the optimal choice for thermal management applications. Phase Change Materials (PCMs) represent the most prominent LHS technology due to their exceptional energy storage capacity during phase transitions (Huang *et al*. 2004).
PCMs are classified based on transition temperature:

- **Low-temperature (<15°C)**
- **Medium-temperature (15–90°C)**
- **High-temperature (>90°C)**

They are also categorized by chemical composition:
Organic PCMs (paraffins, fatty acids):
Advantages: Thermal/chemical stability, resistance to supercooling.
Disadvantages: Low thermal conductivity (0.1–0.3 W/m·K).
Inorganic PCMs (hydrated salts, alloys):
Advantages: Higher thermal conductivity (0.4–0.7 W/m·K), doubled storage capacity.
Disadvantages: Moderate chemical stability.
Eutectic PCMs (multi-component mixtures):
Advantages: Low melting points, stability during phase transition.
Optimal PCM selection requires a comprehensive evaluation of thermal, physical, and chemical properties, alongside economic feasibility. Key criteria include storage capacity, thermal conductivity, chemical stability, heat transfer rates, and overall cost. This holistic framework ensures the selection of the most suitable materials for each application, considering specific environmental and design conditions.
PV panel cooling systems using PCMs (PV-PCM) have evolved significantly since the pioneering study integrating a solar panel with an RT25 PCM system and thermal fins. Results showed a surface temperature reduction from 45°C to below 35°C using a 30-mm PCM layer (Huang *et al*. 2006). These findings stimulated subsequent research exploring diverse PCM types under varying climatic conditions, enhancing the scientific understanding of efficiency mechanisms.
Recent research focuses on enhancing PCM performance via nanomaterial integration. An RT55 system reinforced with 2% Al_2O_3 nanoparticles achieved a 7.1% improvement in daily efficiency (Haghighi *et al*. 2020), while copper (Cu) and silicon carbide (SiC) nanoparticles reduced temperature by 4–5°C with a 4.3% performance enhancement (Luo *et al*. 2017). Studies also indicate that adding 0.5% TiO_2 nanoparticles to paraffin wax can improve panel efficiency by 2.1% alongside a 13°C thermal reduction (Nada *et al*. 2018).

Advanced hybrid systems combining multiple technologies have emerged. A PVT-PCM system achieved a thermal efficiency of 48.5% (Hasan et al., 2015), while integrating ZnO nanofluids (0.2 wt%) with paraffin wax PCM improved energy efficiency by over 23% compared to conventional panels (Huang, 2011). Using a silica/water mixture (3 wt%) with paraffin increased thermal efficiency by 10% (Hosseinzadeh *et al.* 2018). Research also reveals the impact of operational factors: increasing tilt angle (0°–90°) extends PCM melting time while reducing temperature by 0.4–12% (Sardarabadi et al., 2017), whereas top-to-bottom water flow achieves optimal results—reducing temperature by 5.4°C and improving efficiency to 12.4% (Al-Waeli *et al*. 2017). Optimal sequencing of PCMs by melting point can increase melting duration by 18% and thermal efficiency by 33% (AL-Musawi *et al*. 2019). Despite these advancements, PV-PCM systems face technical challenges, including the inherently low thermal conductivity of most PCMs, performance degradation over repeated cycles, the high cost of effective materials, and the complexity of hybrid designs. Current research focuses on developing hybrid nanomaterials to improve thermal conductivity, creating advanced eutectic materials, refining hybrid cooling systems, and establishing accurate mathematical performance models. Collective experimental results indicate that PV-PCM systems represent a promising solution for enhancing PV efficiency, particularly when integrated with supplementary cooling technologies. Continued advancements in nanomaterials and system design herald broader adoption of these technologies in the near future

2. Methodology

2.1 Preparation of Copper Oxide Nanoparticles (CuO NPs)

Copper oxide nanoparticles (CuO NPs) were synthesized via a chemical precipitation method. A total of 4.5 g of copper sulfate pentahydrate ($CuSO_4 \cdot 5H_2O$) was dissolved in 100 mL of absolute ethanol under magnetic stirring at 500 rpm for 10 min at 25 ± 2°C. Subsequently, a separate solution was prepared by dissolving 4.5 g of sodium hydroxide (NaOH) in 200 mL of ethanol. The NaOH solution was gradually added (at a rate of 1 mL/min) to the copper sulfate solution under continuous stirring at 800 rpm. The addition process lasted 60 min while maintaining the temperature at 25 ± 2°C and adjusting the pH to 8.0 ± 0.2.

The mixture was then heated to 80 ± 2°C for 2 h until a dark brown gel formed. The precipitate was filtered and washed multiple times with an ethanol-water mixture (3:1 ratio). The washed precipitate was dried in an oven at 80 ± 5°C for 12 h, followed by calcination in an electric furnace at 400 ± 5°C for 2 h (heating rate: 5°C/min). Finally, the sample was ground for 15 min using an agate mortar and stored in an airtight glass container with silica gel to prevent moisture absorption.

Characterization of CuO NPs:

The properties of the synthesized CuO NPs were determined using the following techniques:

- **X-Ray Diffraction (XRD)**: Analysis was performed using a PANalytical X'Pert PRO MPD diffractometer with Cu Kα radiation (λ = 1.54060 Å).
    - Scanning range (2θ): 20° to 80°
    - Operating conditions: 40 kV voltage, 25 mA current
    - Crystallite size (D_{av}) was calculated using the Debye-Scherrer equation:
- **$D_{av}=0.9\lambda\beta\cos\theta$……(1)**

Where:

β = Full width at half maximum (FWHM) of the peak, λ = X-ray wavelength.

- **Atomic Force Microscopy (AFM)**: Microscopic images were acquired using a Nano Surf microscope to analyze nanoscale particle distribution and surface morphology.

2.2 Effect of Synthesized Copper Oxide on Paraffin Wax Thermal Conductivity

The influence of synthesized CuO NPs on the thermal conductivity of paraffin wax (supplied by Kmart Chemical Technology Company) was investigated. Composite samples were prepared by incorporating varying concentrations of CuO NPs (1, 1.5, 2, 2.5, and 3 wt% relative to the wax mass). Paraffin wax was melted in a water bath at 75°C, after which nanoparticles were added under continuous mechanical stirring until homogeneous dispersion was achieved. The mixture was cast into molds (14 × 14 × 1 cm^3) and allowed to solidify.

Thermal conductivity measurements were conducted using a custom apparatus consisting of:

1. A thermostatically controlled bath with heating resistors
2. Integrated temperature sensors
3. A thermally insulated test chamber for samples.

Both modified (CuO-enhanced) and unmodified paraffin samples were placed in the test chamber. The temperatures of the upper and lower surfaces were monitored by direct-contact thermal sensors. Thermal conductivity (*k*) was calculated according to Fourier's Law (Equation 2), as illustrated in **Figure 1**:

$$\mathbf{Q} = \frac{(\mathbf{K} * \mathbf{A} * \Delta\mathbf{T})}{\mathbf{d}} \ldots\ldots\ldots (\mathbf{2})$$

Where:

Q: Heat transfer rate (W)

k: Thermal conductivity coefficient (W/m·K)

A: Cross-sectional area of the sample (m^2)

ΔT: Temperature difference between sample surfaces (K or °C)

d: Sample thickness (m)

The heat transfer rate Q was calculated using Equation (3):

$$\mathbf{Q} = \mathbf{I} * \mathbf{V} \ldots\ldots\ldots\ldots (\mathbf{3})$$

Where:

I: Current intensity (A)

V: Voltage (V)

The thermal conductivity enhancement percentage (k) of the nano-CuO/paraffin phase change material (PCM) composite was calculated using the following equation:

$$\mathbf{K}_{\%} = \frac{\mathbf{K}_{\mathbf{Nanopcm}} - \mathbf{K}_{\mathbf{Paraffin}}}{\mathbf{K}_{\mathbf{Paraffin}}} \ldots\ldots\ldots\ldots (\mathbf{4})$$

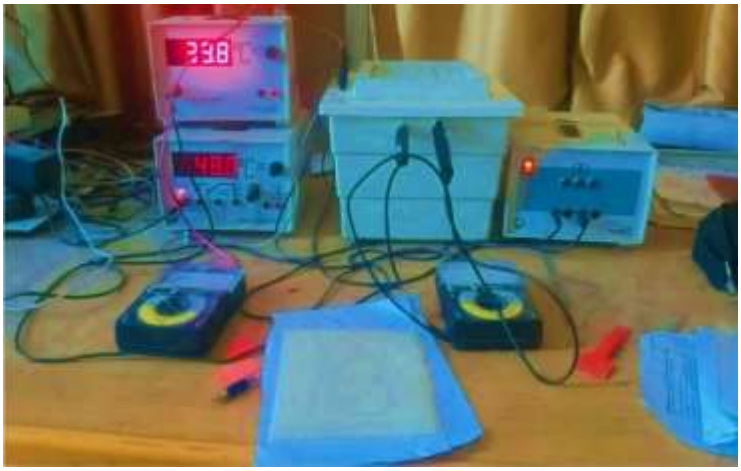

Figure 1. Thermal Conductivity Measurement

2.3. Solar Panel Performance Evaluation Criteria

Photovoltaic Conversion Efficiency

The solar panel efficiency (η) represents the ratio of the maximum electrical power output (P_{max})to the incident solar energy on the panel surface, expressed by the equation:

$\eta = (V_m \times I_m) / (E \times A) \times 100\%$ … (5)

Where:

V_m and I_m: Voltage and current at the maximum power point (MPP)

***E*:** Solar irradiance (W/m²)

***A*:** Effective panel area (m²)

Efficiency is significantly influenced by panel temperature, as *V*_m decreases with rising temperature according to the temperature coefficient.

Fill Factor (FF)

The fill factor serves as an indicator of solar cell quality, calculated as the ratio of the theoretical maximum power ($P_o=V_{oc}\cdot I_{sc}$) to the actual maximum power output (Pmax):

$FF=P_{max}/Po = V_m \cdot I_m / V_{oc} \cdot I_{sc}$ … (6)

Where:

V_{oc}: Open-circuit voltage

I_{sc}: Short-circuit current

The fill factor (FF) is inversely proportional to temperature due to reduced V_{oc}, making it a sensitive criterion for performance assessment under varying operational conditions.

Normalized Power Output Efficiency

The normalized power output efficiency is defined as the ratio of measured output power under actual conditions to that measured under standard test conditions (STC). This efficiency is calculated as a percentage using the following equation:

$$\textbf{Normalized Power Output Efficiency} = \frac{P_{actual}}{P_{stc}} \times 100 \ldots\ldots (7)$$

Where:

P_{actual}: Electrical power output (W) measured under real operating conditions (site-specific irradiance, temperature, and environmental factors)

P_{stc} : Electrical power output (W) measured under Standard Test Conditions (STC: 1000 W/m², 25°C cell temperature, AM 1.5 spectrum)

2.4 Test Model Design

Monocrystalline silicon solar panels (General Gold Co.) with dimensions 67 × 44.5 × 1.7 cm and rated power 50 W were employed. The panels featured an open-circuit voltage (V_{oc}) of 22 V and short-circuit current (I_{sc}) of 3 A. An aluminum containment unit (64 × 42 × 2.5 cm) housing the nano-enhanced paraffin wax was thermally coupled to the rear surface of each panel.

The PV modules were mounted at a 33° tilt angle facing south to maximize solar irradiance exposure. Temperature monitoring was performed using Weewooday K-type thermocouples strategically positioned across the panel surface to calculate the average PV module temperature for each measurement interval. Voltage and current measurements were recorded with a DT830B digital multimeter (operational ranges: 200 mV–2000 V DC, 200 μA–10 A).

Electrical power output was calculated using Equation (8). Experiments were conducted over three consecutive days with 9-hour daily monitoring periods (08:00–17:00 local time):

$$\textbf{Pmax} = \textbf{Imax} * \textbf{Vmax} \ldots\ldots (8)$$

Where:

- **Pmax**: Maximum generated power (W)
- **Imax**: Maximum current (A)
- **Vmax**: Maximum voltage (V)

The average power variation for each test case was determined using Equation (9):

$$\Delta P = \frac{P_{max2} - P_{max1}}{p_{max1}} * 100 \ldots\ldots\ldots\ldots (9)$$

Where:

- **P_{max2}: Maximum power output of modified solar panel**
- **P_{max1}: Maximum power output of reference solar panel**

3. Results and Discussion

3.1 Characterization of Copper Oxide Nanoparticles (CuO NPs)

The X-ray diffraction (XRD) pattern of synthesized copper oxide nanoparticles (CuO NPs) in **Figure 2** exhibits characteristic peaks at diffraction angles (2θ) between 20° and 80°. These peak positions precisely match the (hkl) crystallographic planes of copper oxide (JCPDS card no. 05-0661). The most prominent peak at 35.5° corresponds to the (1̄11) plane, while other distinctive peaks appear at 38.7° (111), 48.7° (202), 58.3° (113), and 61.5° (311), collectively confirming the monoclinic tenorite structure of CuO.

Crystallite size was estimated at 18-25 nm through Scherrer equation analysis of the dominant (1̄11) peak using Cu Kα radiation (λ = 1.5406 Å) and the full width at half maximum (FWHM). Peak broadening indicates the nanoscale nature of the material, while symmetrical peak profiles confirm homogeneous particle size distribution.

The absence of extraneous peaks demonstrates high sample purity with no detectable secondary phases (e.g., Cu_2O or metallic Cu). Minimal baseline scattering further confirms the absence of amorphous components. The measured diffraction angles show precise alignment with reference data for phase-pure CuO, confirming successful synthesis.

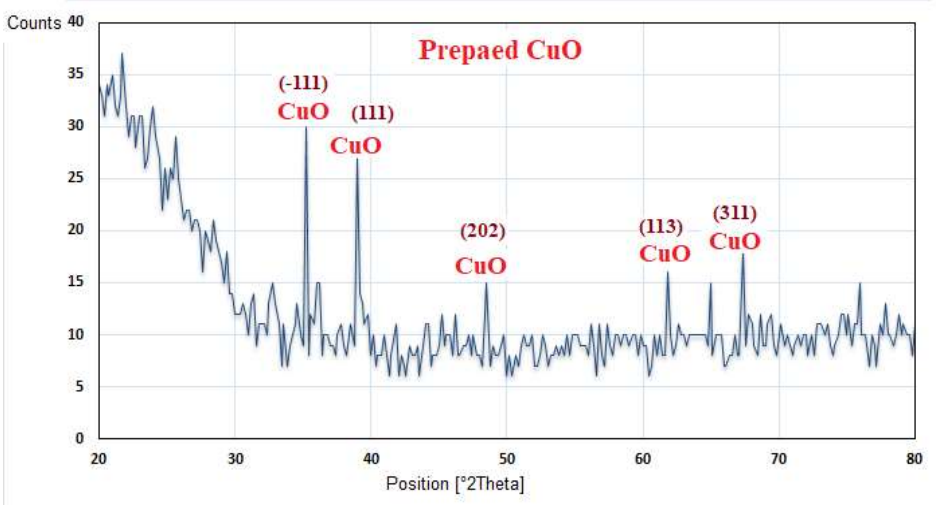

Figure 2. X-ray diffraction (XRD) pattern of synthesized copper oxide nanoparticles (CuO NPs) prepared via chemical precipitation.

Figure 3 presents two-dimensional (2D) and three-dimensional (3D) atomic force microscopy (AFM) images of copper oxide nanoparticles (CuO NPs), revealing distinctive surface characteristics

that confirm the nanoscale nature of the material. The 3D image shows homogeneous nanoscale aggregates uniformly distributed across the surface, with topographic heights ranging from -45 nm to +50 nm. This indicates relative surface smoothness with localized nanoprotrusions.

The 2D image demonstrates uniform nanoparticle distribution across a 5 × 5 µm scan area, exhibiting fine surface topography indicative of nanoscale roughness. The limited and homogeneous surface roughness confirms particle sizes within the nanoscale regime (<100 nm).

Surface roughness analysis yielded low values (within several nanometers), consistent with monodisperse nanoparticles. The absence of large topographic features or deep voids confirms minimal particle aggregation and no surface contaminants.

These AFM-derived characteristics - including particle distribution, height variation, and roughness parameters - provide compelling evidence of successful CuO NP synthesis with excellent size homogeneity and surface distribution. These findings align with XRD crystallite size analysis (18-25 nm), confirming synthesis consistency across characterization techniques.

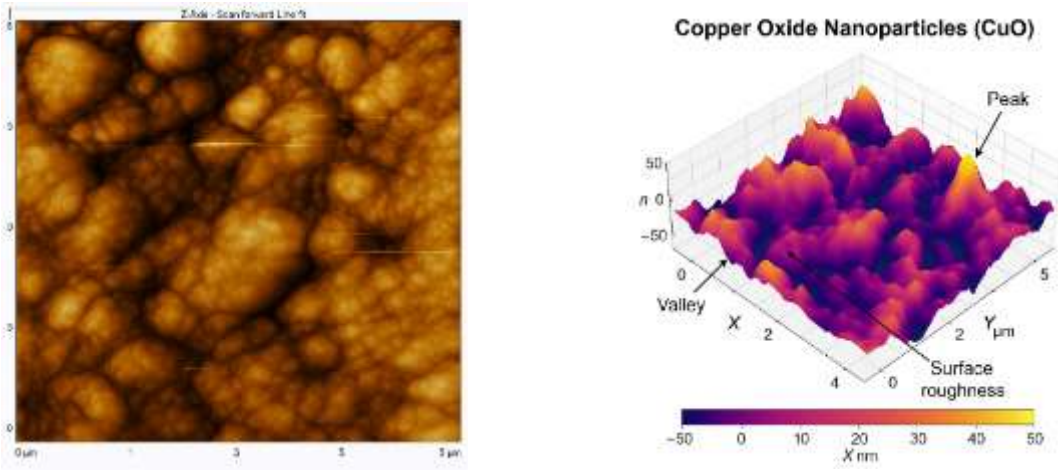

Figure 3. Atomic Force Microscopy (AFM) 2D and 3D images of Copper Oxide Nanoparticles (CuO NPs)

3.2 Effect of Copper Oxide Nanoparticles (CuO NPs) on Paraffin Wax Thermal Conductivity

As presented in **Table 1**, incorporating copper oxide nanoparticles (CuO NPs) significantly enhanced the thermal properties of paraffin wax. The baseline thermal conductivity of unmodified paraffin wax measured 0.4857 W/m·K. With the addition of 0.5 wt% nanoparticles, thermal conductivity increased substantially to 1.12 W/m·K, representing a 130.6% enhancement relative to the reference sample.

A positive correlation between nanoparticle concentration and thermal conductivity was observed up to 2 wt%, where peak thermal conductivity reached 2.34 W/m·K (381.8% improvement). However, increasing the concentration to 2.5 wt% reduced thermal conductivity to 1.57 W/m·K. This reduction is attributed to nanoparticle agglomeration and heterogeneous dispersion within the wax matrix, as evidenced by microscopic observations revealing non-uniform brown patches on sample surfaces.

These results indicate an optimal nanoparticle loading of 2 wt%, which maximizes thermal conductivity enhancement while maintaining homogeneous particle distribution. The thermal improvement mechanisms include:

1. **Inherent high thermal conductivity** of CuO nanoparticles
2. **Formation of efficient thermal networks** at optimal concentrations
3. **Enhanced interfacial interactions** between nanoparticles and wax molecules

Table 1. **Influence of copper oxide nanoparticle concentration on thermal conductivity of paraffin wax**

Thermal conductivity (W/m.K)	CuO NPs (wt%)	Paraffin(wt%)
0.4857 ± 0.02	0	100
1.12 ± 0.03	0.5	99.5
1.35 ± 0.04	1	99
1.89 ± 0.05	1.5	98.5
2.15 ± 0.06	2	98
1.57 ± 0.07	2.5	97.5

Figure 4 data demonstrate a significant thermal conductivity enhancement of 381.8% at the optimal concentration (2 wt%), with a pronounced reduction observed at higher concentrations due to nanoparticle agglomeration phenomena. These findings provide critical insights for designing thermally enhanced phase change materials (PCMs), highlighting the necessity for precise control of nanofiller loading concentrations to achieve an optimal balance between thermal conductivity improvement and homogeneous dispersion stability.

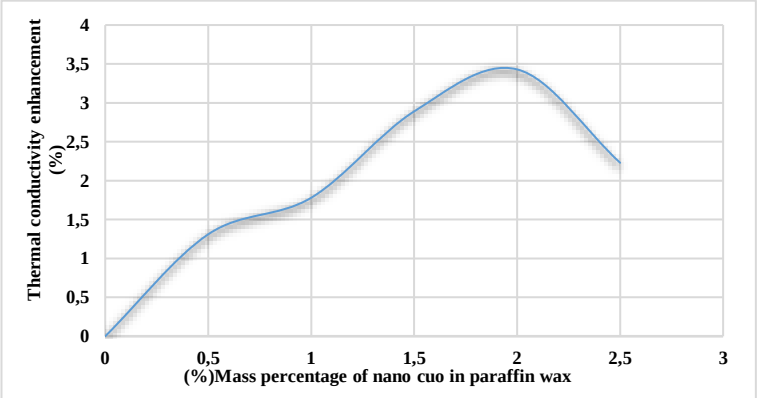

Figure 4. **Effect of copper oxide nanoparticles on thermal conductivity of paraffin wax**

3-3-Temperature Effect on Photovoltaic Panel Performance (Without Cooling System)

The uncooled reference panel exhibited significant performance degradation under elevated temperatures during harsh July conditions. At solar noon (12:00) with 1025 W/m² irradiance, the panel surface temperature peaked at 77.1°C. This thermal stress reduced output voltage to 15.25 V (compared to the nominal 22V), demonstrating the direct adverse impact of temperature rise on photovoltaic properties. The degradation manifested as a 42% efficiency loss, with maximum power output limited to 28.82 W. Temperature elevation adversely affected the cell fill factor (FF), diminishing energy conversion efficiency through increased internal resistance **Table 2.**

3-4-Temperature Effect on Photovoltaic Panel Performance with Paraffin Wax-Based Cooling System

Experimental results from the PCM-integrated system (18 July 2024) in **Table 3** demonstrated significant thermal and electrical performance improvements compared to the reference panel. The phase-change cooling system effectively reduced surface temperatures during peak solar irradiance, with the cooled panel reaching a maximum temperature of 66.12°C at noon versus 77.1°C for the reference panel - representing a 14.2% reduction under identical 1025 W/m² irradiance. This thermal mitigation is attributed to paraffin's latent heat absorption during phase transition, which diminished heat transfer to PV cells.

This thermal enhancement positively influenced electrical properties, increasing output power by 23.8% (35.69 W vs. 28.82 W for the reference panel during identical periods). The improvement resulted from optimized voltage and current coefficients at lower temperatures, evidenced by higher operational voltage (15.79 V vs. 15.25 V at noon). This voltage elevation confirms the detrimental impact of temperature elevation on monocrystalline semiconductor properties.

These findings underscore the critical need for active cooling systems in high-irradiance regions, highlighting thermal management's essential role in achieving:

1. Output voltage stabilization,
2. Thermal loss minimization,
3. Overall efficiency optimization.

Table 2. Temperature Effect on Photovoltaic Panel Performance (Without Cooling System)

Power Output (W)	Current (Amp)	Voltage (V)	Panel Temperature (°C)	Ambient Temperature (°C)	Solar Irradiance (W/m²)	Time (Hour)
8.91	0.67	13.3	41	27	370	**08:00**
13.20	0.96	13.75	50	29.5	505	**09:00**
20.15	1.37	14.71	60.5	34	710	**10:00**
25.98	1.73	15.02	71	36.7	900	**11:00**
28.82	1.89	15.25	77.1	37.4	1025	**12:00**
26.91	1.78	15.12	72.01	37.7	975	**13:00**
23.05	1.57	14.68	65.12	36.2	790	**14:00**
17.51	1.25	14.01	56.5	39.82	615	**15:00**
12.02	0.89	13.50	48.12	31.90	444	**16:00**

Table 3. Temperature Effect on Photovoltaic Panel Performance with Paraffin Wax-Based Cooling System

Power Output (W)	Current (Amp)	Voltage (V)	Temperature Reduction (°C)	Panel Temperature (°C)	Time (Hour)
11.35	0.85	13.35	2.70	38.3	**08:00**
17.22	1.24	13.89	5.35	44.65	**09:00**
23.94	1.63	14.69	8.12	52.38	**10:00**
31.24	2.08	15.02	10.01	60.99	**11:00**
35.69	2.26	15.79	10.98	66.12	**12:00**
33.88	2.19	15.47	10.33	61.68	**13:00**
26.88	1.82	14.77	8.99	56.13	**14:00**
21.13	1.48	14.28	7.80	48.4	**15:00**
13.94	1.02	13.67	6.13	41.99	**16:00**

3.5 Performance Impact of Hybrid Cooling System (Paraffin Wax + CuO Nanoparticles) on Photovoltaic Modules

Table 4 presents performance data for the system integrated with nano-enhanced paraffin (PCM/CuO NPs, k = 2.15 W/m·K) recorded on 18 July 2024, demonstrating superior thermal regulation and electrical output compared to conventional systems. The nano-enhanced panel achieved a peak surface temperature of 55.3°C at solar noon under 1025 W/m² irradiance, versus 66.12°C for the pure paraffin-cooled panel - representing an additional 16.36% temperature reduction. This improvement is attributed to the enhanced thermal conductivity of copper oxide nanoparticles, which optimized latent heat transfer within the phase change material.

This advanced cooling significantly improved electrical parameters: peak power output reached 37.21 W compared to 35.69 W for the unenhanced paraffin system (4.3% enhancement). Concurrently, maximum voltage increased to 16.25 V versus 15.79 V (2.9% increase), demonstrating improved semiconductor performance at lower operating temperatures. **Table 5** compares the performance of standard photovoltaic modules versus those integrated with the hybrid cooling system (paraffin wax reinforced with copper oxide nanoparticles).

Table 4. Performance Impact of Hybrid Cooling System (Paraffin Wax + CuO Nanoparticles) on Photovoltaic Modules

Power Output (W)	Current (Amp)	Voltage (V)	Temperature Reduction (°C)	Panel Temperature (°C)	Time (Hour)
11.32	0.76	14.9	4.5	36.50	**08:00**
17.29	1.13	15.3	9	41.00	**09:00**
23.96	1.52	15.76	13.5	47.00	**10:00**
31.28	1.97	15.88	17.3	53.70	**11:00**
37.21	2.29	16.25	21.80	55.3	**12:00**
33.53	2.08	16.12	20.12	51.89	**13:00**
27.00	1.71	15.79	18.20	46.92	**14:00**
21.24	1.37	15.5	15.01	41.49	**15:00**
13.89	0.92	15.1	10.2	37.92	**16:00**

Table 5. Performance of the paraffin-based cooling panel enhanced with copper oxide nanoparticles PCM/CuO NPs compared to the reference panel.

Time	Temperature (°C)	Thermal Change (°C)	Voltage (V)	Current (A)	Power Output (W)	Power Improvement (%)
08:00	36.50 (-4.50)	-4.50	14.90 (+1.60)	0.76 (+0.09)	11.32	+27.0%
12:00	55.3 (-21.80)	-21.80	16.25 (+1.00)	2.29 (+0.40)	37.21	+29.1%
16:00	37.92 (-10.20)	-10.20	15.10 (+1.60)	0.92 (+0.03)	13.89	+15.6%

Note: Values in parentheses represent the change relative to the reference panel.

Physical analysis revealed that the cooling mechanism relies on nanoparticle-induced enhancement of the phase change material's thermal conductivity from 0.4857 W/m·K to 2.15 W/m·K. The homogeneous distribution of nanoparticles at 2 wt% concentration establishes efficient thermal percolation networks. The high surface-to-volume ratio of nanoparticles significantly improved interfacial heat transfer (Byiringiro *et al.*, 2025b).

From an electro-thermal perspective, temperature reduction enhanced P-N junction characteristics by:

1. Decreasing minority carrier concentrations
2. Suppressing reverse leakage current
3. Improving cell fill factor by 5.9%

Performance analysis demonstrated peak efficiency enhancement from 9.44% to 12.18% (29% relative gain), with 22.75% improvement in daily energy yield. These results confirm the system's efficacy in photovoltaic performance optimization through precise thermal management, achieving:

- Output voltage stabilization
- Thermal loss minimization
- Operational reliability enhancement

Conclusion

This study has achieved tangible scientific progress in enhancing the efficiency of photovoltaic systems through the development of an innovative cooling system based on phase change materials (PCMs) enhanced with nanoparticles. The results demonstrated the successful synthesis of copper oxide nanoparticles (CuO NPs) with a pure crystalline structure and homogeneous size distribution between 18-25 nm, as confirmed by XRD and AFM analyses. Upon integrating these nanoparticles at 2% by weight with paraffin wax, a hybrid material was developed that exhibited qualitative improvement in thermal properties, manifested in a 381.8% increase in thermal conductivity compared to the base material.

The developed cooling system proved highly efficient in thermal control, recording an average reduction in operating temperature of 14.4°C, while achieving a maximum thermal reduction of 21.80°C under peak irradiance conditions. This thermal improvement translated into substantial enhancements in photovoltaic performance, represented by a 29.11% increase in maximum power output, a rise in peak efficiency from 9.44% to 12.18%, and a boost in daily energy yield of 22.75%. The fundamental mechanisms underlying these improvements lie in the formation of effective thermal conductive networks, enhancement of latent heat transfer dynamics, and reduction of thermal loss at the P-N junction.

These findings open new horizons for developing sustainable solutions in thermal management for renewable energy applications, with the potential for expansion into studying multi-component hybrid nanocomposites, developing precise mathematical models, and assessing the economic feasibility for large-scale industrial implementation.

Acknowledgement, the authors gratefully acknowledge the support provided by the University of Aleppo.

Disclosure statement: *Conflict of Interest:* The authors declare that there are no conflicts of interest.
Compliance with Ethical Standards: This article does not contain any studies involving human or animal subjects.

References

AL-Musawi A.I.A., Taheri A., Farzanehnia A., Sardarabadi M., Passandideh-Fard M. (2019) Numerical study of the effects of nanofluids and phase-change materials in photovoltaic thermal (PVT) systems. *Journal of Thermal Analysis and Calorimetry*, 137(2), 623-636. https://doi.org/10.1007/s10973-018-7972-6

Al-Waeli A.H.A., Sopian K., Chaichan M.T., Kazem H.A. (2017) Evaluation of the nanofluid and nano-PCM based photovoltaic thermal (PVT) system: An experimental study. *Energy Conversion and Management*, 151, 693-708. https://doi.org/10.1016/j.enconman.2017.09.032

Armstrong S., Hurley W.G. (2010) A thermal model for photovoltaic panels under varying atmospheric conditions. *Applied Thermal Engineering*, 30(11-12), 1488-1495. https://doi.org/10.1016/j.applthermaleng.2010.03.012

Baloch A.A.B., Bahaidarah H.M.S., Gandhidasan P. (2015) An experimental study of the effect of converging channel heat exchanger on PV system. In: *2015 IEEE 42nd Photovoltaic Specialist Conference (PVSC)*, New Orleans, LA, USA, pp. 1-4. https://doi.org/10.1109/PVSC.2015.7356010

Byiringiro J., Chaanaoui M., Hammouti B. (2025a) Thermal performance enhancement of a novel receiver for parabolic trough solar collector. *Interactions*, 246, 13. https://doi.org/10.1007/s10751-024-02230-3

Byiringiro J., Chaanaoui M., Hammouti B. (2025b), Enhancement of thermal performance in parabolic trough solar Collectors: Investigation of three novel receiver configurations using advanced heat transfer fluids, *Solar Energy Materials and Solar Cells*, 293, 113833, ISSN 0927-0248, https://doi.org/10.1016/j.solmat.2025.113833

Domański M.J., Rebow M. (1995) Thermal energy storage problems. *Journal of Power Technologies*, 79, 25-35.

Dwivedi P., Sudhakar K., Soni A., Solomin E., Kirpichnikova I. (2020) Advanced cooling techniques of PV modules: a state of art. *Case Studies in Thermal Engineering*, 21, 100674. https://doi.org/10.1016/j.csite.2020.100674

Haghighi A., Babapoor A., Azizi M., Javanshir Z., Ghasemzade H. (2020) Optimization of the thermal performance of PCM nanocomposites. *Journal of Energy Management and Technology*, 4(2), 14-19. https://doi.org/10.22109/JEMT.2019.152458.1134

Haidar Z.A., Orfi J., Kaneesamkandi Z. (2018) Experimental investigation of evaporative cooling for enhancing photovoltaic panels efficiency. *Results in Physics*, 11, 690-697. https://doi.org/10.1016/j.rinp.2018.10.016

Han X., Wang Q., Zheng J. (2016) Determination and evaluation of the optical properties of dielectric liquids for concentrating photovoltaic immersion cooling applications. *Solar Energy*, 133, 476-484. https://doi.org/10.1016/j.solener.2016.04.036

Hasan A., McCormack S., Huang M., Sarwar J., Norton B. (2015) Increased photovoltaic performance through temperature regulation by phase change materials: Materials comparison in different climates. *Solar Energy*, 115, 264-276. https://doi.org/10.1016/j.solener.2015.02.003

Hosseinzadeh M., Sardarabadi M., Passandideh-Fard M. (2018) Energy and exergy analysis of nanofluid based photovoltaic thermal system integrated with phase change material. *Energy*, 147, 636-647. https://doi.org/10.1016/j.energy.2018.01.073

Huang M.J., Eames P.C., Norton B. (2011) Two phase change material with different closed shape fins in building integrated photovoltaic system temperature regulation. *Linköping Electronic Conference Proceedings*, (63), 2938-2945. http://dx.doi.org/10.3384/ecp110572938

Huang M., Eames P., Norton B. (2004) Thermal regulation of building-integrated photovoltaics using phase change materials. *International Journal of Heat and Mass Transfer*, 47(12-13), 2715-2733. https://doi.org/10.1016/j.ijheatmasstransfer.2003.11.015

Huang M., Eames P., Norton B. (2006) Phase change materials for limiting temperature rise in building integrated photovoltaics. *Solar Energy*, 80(9), 1121-1130. https://doi.org/10.1016/j.solener.2005.10.006

Huang M., Eames P., Norton B., Hewitt N. (2011) Natural convection in an internally finned phase change material heat sink for the thermal management of photovoltaics. *Solar Energy Materials and Solar Cells*, 95(7), 1598-1603. https://doi.org/10.1016/j.solmat.2011.01.008

Indartono Y.S., Suwono A., Pratama F.Y. (2016) Improving photovoltaics performance by using yellow petroleum jelly as phase change material. *International Journal of Low-Carbon Technologies*, 11(3), 333-337. https://doi.org/10.1093/ijlct/ctu033

Khanna S., Reddy K.S., Mallick T.K. (2018) Optimization of finned solar photovoltaic phase change material (finned PV PCM) system. *International Journal of Thermal Sciences*, 130, 313-322. https://doi.org/10.1016/j.ijthermalsci.2018.04.033

Luo Z., Wang R., Xiao C., Zhang Y., Chen H. (2017) Numerical and experimental study on temperature control of solar panels with form-stable paraffin/expanded graphite composite PCM. *Energy Conversion and Management*, 149, 416-423. https://doi.org/10.1016/j.enconman.2017.07.046

Nada S., El-Nagar D., Hussein H. (2018) Improving the thermal regulation and efficiency enhancement of PCM-Integrated PV modules using nano particles. *Energy Conversion and Management*, 166, 735-743. https://doi.org/10.1016/j.enconman.2018.04.035

Pal P., Nayak A.K., Dev R. (2018) A modified double slope basin type solar distiller: experimental and enviro-economic study. *Evergreen*, 5(1), 52-61. https://doi.org/10.5109/1929730

Rajaram R., Sivakumar D. (2015) Experimental investigation of solar panel cooling by the use of phase change material. *Journal of Chemical and Pharmaceutical Sciences*, 9, 2115-2120.

Rouf R.A., Khan M.A.H., Kabir K.M.A., Saha B.B. (2016) Energy management and heat storage for solar adsorption cooling. *Evergreen*, 3(2), 1-10. https://doi.org/10.5109/1800866

Sardarabadi M., Passandideh-Fard M., Maghrebi M.J., Ghazikhani M. (2017) Experimental study of using both ZnO/water nanofluid and phase change material (PCM) in photovoltaic thermal systems. *Solar Energy Materials and Solar Cells*, 161, 62-69. https://doi.org/10.1016/j.solmat.2016.11.032

Soudi N., Nanayakkara S., Jahed N.M.S., Naahidi S. (2020) Rise of nature-inspired solar photovoltaic energy convertors. *Solar Energy*, 208, 31-45. https://doi.org/10.1016/j.solener.2020.07.048

Stritih U. (2016) Increasing the efficiency of PV panel with the use of PCM. *Renewable Energy*, 97, 671-679. https://doi.org/10.1016/j.renene.2016.06.011

Tewari K., Dev R. (2018) Analysis of modified solar water heating system made of transparent tubes & insulated metal absorber. *Evergreen*, 5(1), 62-72. https://doi.org/10.5109/1929731